Structural, Morphological, and Spectroscopical Properties of Fullerenes (C60) Thin Film Prepared via Electrospray Deposition

Journal of Physics: Conference Series **1829** (2021) 012018 doi:10.1088/1742-6596/1829/1/012018

Structural, Morphological, and Spectroscopical Properties of Fullerenes (C60) Thin Film Prepared via Electrospray Deposition

Ban M A Alani[1] and Mazin A Alalousi[2]

[1]College of Veterinary Medicine, University of Fallujah, Iraq
[2]Department of Physics, College of Science, University of Anbar, Iraq

E-mail: Banscince2@gmail.com, mazin_alalousi@uoanbar.edu.iq

Abstract. In this study, fullerenes (C_{60}) thin film was prepared via a novel combination of laser pulsed and electrospray methods using wasted batteries' electrodes as precursor. The effect of the applied electric potential using electrospray process was investigated through the structural, morphological and optical analyses. These in turn were examined using x-ray diffraction, field emission scanning electron microscopy, energy dispersive spectroscopy, and photoluminescence techniques. In particular, using Williamson-Hall relation, the average crystallite size of the prepared nanoparticles was estimated in which it was found in the range of 41.46-111.84 nm. While sample treated with 5.6 kV of electric potential exhibited particle size of 6.35 nm using FESEM technique as compared to 7.4 nm for sample prepared under free potential. It is believed that the applied electric potential plays a vital role in reducing the particle size which in turn provides an alternative pathway for fabricating future optoelectronic design.

Keywords: fullerenes (C_{60}), thin film, wasted batteries' electrodes, electrospray

1. Introduction

Modifications of carbon, including different types of fullerenes, diamond, graphene, graphite, amorphous carbon, carbon nanotubes carbon dots, carbon aerogels, and several nano-designed fullerenes, have shown an extensive investigation in the field of nanotechnology[1,2]. This is mainly due to their unique physical and chemical properties such as pore size distributions, tunable porous structure, good mechanical and thermal stability, and high electrical conductivity; thereby each carbon type exhibits different features depending on its size and structure[3]. Unlike graphene and/or graphite, which are assumed as planar geometries in the stable form, fullerene has spherical shape and a pyramidalization angle ($\theta_{\sigma\pi} - 90$) in which the latter depends on the total atoms number of carbon; this particular pyramidalization angle forces the fullerene atoms to form a particular spherical geometry[4,5]. Among several types of fullerene, C_{60} is considered the most stable and commonly known type because of its well-implemented photo-physical and electron-accepting characteristics such as fast electron separation and transportation and high surface-to-volume ratio. Therefore, C_{60} has growing interest in various fields; for instance, nano-electronics[6],

hydrogen storage [7], supercapacitors [8], and biomedical applications including drug and gene delivery[9].

Thin film technology of C_{60} deposited on variety of substrates is being extensively investigated for wide-range of applications. However, the deposited C_{60} film is chemically unstable and fragile which could be attributed to the C_{60} weak crystal formation by van der Waal's force at room temperature[10,11]. Herein, in order to examine the C_{60} layers feasibility, it is of crucial importance to acquire more stable and stronger C_{60} films taking into consideration the initial physical and chemical characteristics. Therefore, a number of deposition techniques have been reported including poor solvent immersion[12], vacuum thermally evaporated[13], droplet [14], dip-coating[15], spin-coating[16], and Langmuir-Blodgett[17]. Among of these techniques[18], the electrospray technique under a precise and controlled electric field effect facilitates precise control of size and motion of the charged droplets by means of the applied voltage and which results in a homogeneous film formation[19].

This attempt reports the preparation of fullerenes (C_{60}) thin film via electrospray deposition process in conjunction with laser pulse technique using wasted batteries' electrodes as precursors. Furthermore, the structural, morphological, and optical properties of the resultant films are systematically investigated as a function of different applied electric potential values.

2. Materials and methods

2.1. Preparation of fullerenes (C_{60}) nanoparticles

The raw materials were obtained from wasted batteries' carbon electrodes, where the collected electrodes were smashed and continuously washed using ethanol then double distilled water (DDDW). The attained powder was grinded and thermally treated using a muffle furnace at 1000 °C for 60 min with a heating rate of 5 °C/min. Subsequently, the thermally treated powder was compressed under 400 bars to obtain 1 cm pellet thickness. Hereinafter, using pulsed Nd-YAG laser, the prepared pellet was immersed in 100 ml of DDDW with height of 8 mm placed on a rotary with a speed of 2 cycles /min. The target, pellet, was pumped using a pulsed Nd-YAG laser with a wavelength of 1064 nm and energy of 100 mJ. The duration and width of pulses were 6 Hz and 10 nm, respectively.

2.2. Deposition of fullerenes (C_{60}) thin film

During the deposition process, p-type silicon (Si) wafer with low resistance was used as substrate; in which the pre-introduced Si wafer was cut into specific dimensions$(1.5 \times 1.5)cm$. The substrate was multi-washed using solution of HF acid diluted with DDDW (1:10 HF: H_2O) in ultrasonic bath for 5 min. Simultaneously, the carbon colloid was sprayed vertically on the Si waver which in turn was placed on a hot plate (250 °C) with height of 30 cm from the jet nozzle (Figure 1). The on/off spraying time was maintained at 5 and 12 sec respectively, with variety of applied DC electrical potential (0, 4, 5, and 5.6 kV). In order to ensure high crystallization process and avoid the occurrence of crystal defects, the Si waver was left for $15\ min$ once the spray process completed.

The structural property of fullerenes (C_{60}) was performed on x-ray diffractometer (XRD-6000) using CuKα radiation and accelerated voltage of 40 kV. In the meanwhile, a field emission scanning electron microscope (FESEM, INSPECT-550) 5.00 KV was introduced to investigate the homogeneous distribution as well as the surface morphology of the deposited films. In conjunction with the FESEM technique, the element composition analysis and purity of the prepared materials were perceived using EDX spectrometer (Bruker X Flash 6L10). Finally, the optical behavior of the deposited films was systematically studied on Perkin-Elmer LS-50B luminescence spectrophotometer.

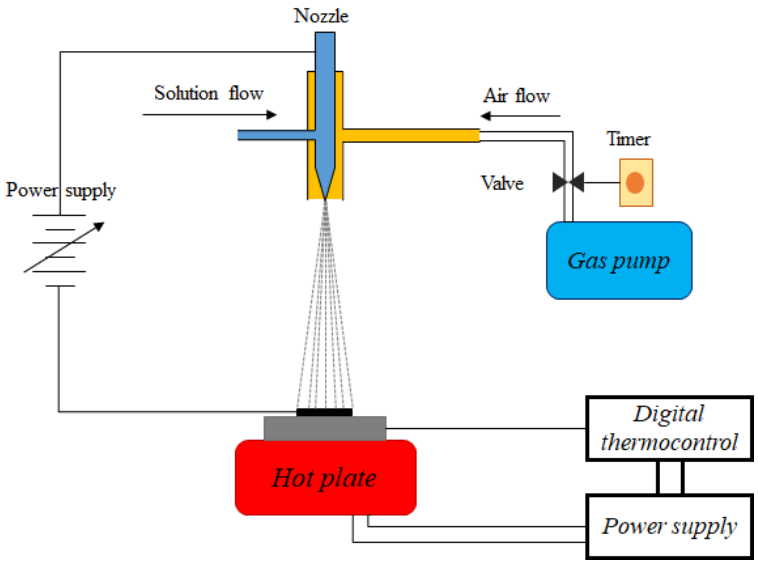

Figure 1: Schematic representation of the electrospray technique setup with the applied electric potential.

3. Results and discussion

The XRD analysis was performed to acquire a general observation of the structural formation of the deposited fullerenes (C_{60}) thin films. In particular, the films prepared without the effect of electric potential showed a dominant peak at 27.9^{o} which can mainly be indexed to the formation of C_{60} crystal structure with orientation of (220) (Figure 2, a). Moreover, it can also be clearly noticed that some peaks indicated the occurrence of C_{60}-polymeric structure as well as Graphite; where the polymerization of C_{60} could be attributed to the colloidal synthesis occurred within the deposition process. This in turn mainly depends on the generation of high-pressure plasma cloud during the reaction between the laser beam and the target and/or the nanoparticles[5]. Continuously, Figure 2 (b) presents the effect of the applied electric potential (4 KV) throughout the deposition process. It can be observed from the Figure that the dominant peak is located at 69.5° which can be indexed to the C_{60} crystal formation with (446) of orientation; additional two peaks were also noticed corresponded to the occurrence of $C_{60}H_{34}$ (hartite). The latter could be due to the bonding between the C_{60} shell and hydrogen atoms caused by heat and the electric field[2]. It is worth mentioning that the aforementioned process resulted in C_{60} peak intensity reduction and some deformation was attained. The effect of 5 KV electric potential on the deposition process is illustrated in Figure 2,c in which it is obvious that the dominant peak of C_{60} is located at 28.45° with orientation of (123). Furthermore, the applied electric field resulted in the disappearance of hartite phase and subsequently the of C_{60}-polymeric peak at 79.30°. However, both hexagonal carbon and C_{60}-polymeric phases were noticed upon applying 5.6 KV electric potential alongside the C_{60} crystal formation noticed at $2\theta = 28.10°$ (Figure 2, d). Generally, the results obtained (Figure 2, a-d) are in a good agreement, to a certain extent, with previously published data [2,5]. Additionally, the crystallite size of the demonstrated samples was estimated based on the Williamson-Hall relation[20].

$$D = \left(\frac{k\,\lambda}{\beta_{hkl}\,cos\theta}\right) + (4\varepsilon \sin\theta) \quad (1)$$

Where D (nm) is the crystalline size, k is dimensionless shape factor (0.89), λ is the wavelength radiation of the used X-ray (nm), $\beta_{hkl}$is the full width at half maximum (FWHM) of the diffraction peaks, and θ (rad) is the radian diffraction angle.

In the meanwhile, the crystallinity indices ($X_{C.I}$) were also calculated [21]; the corresponded outcomes are tabulated in Table 1. Under no electric potential effect, both average of crystalline size and $X_{C.I}$ were affected by the applied electrical potential that found to be 111.84 nm, while $X_{C.I}$ is 98.9%, where C_{60} is about 99.46% based on the intensity ratio (RIR) method.

The surface morphologies of the deposited films are investigated using FESEM technique for which Figure 3 (a-h) is illustrated. The deposited film under free potential revealed the occurrence of nano-porous structure with clusters size ranging from 29 to 890 nm; particularly, these clusters were formed by average particle size of $7.4 \mp 0.06\ nm$ and film thickness of $196.8\ nm$ (Figure 3, (a and b)). The acquired nano-porous structure was decreased in size under the effect of 4 KV electric potential in which the size range was estimated as $47 - 235\ nm$ (Figure 3 (c and d)); the average particle size was found to be $6.65 \pm 0.08\ nm$ with film thickness of $272.25\ nm$. This can be explained by the droplets separation phenomenon in which the applied electric potential during the electrospray process results in separation of droplets produced from the jet nozzle and subsequently the production of small nanoparticles which eventually assembled on hot plate to form clusters [21]. Subsequently, in Figure 3 (e and f), a coral reefs structure was perceived under electric potential of 5 KV which exhibited cluster size ranging from 51.5 up to $153.5\ nm$ and average particle size of 6.35 ± 0.06 and $357\ nm$ film thickness. These morphological properties could be related to the C_{60} phase dominance as previously discussed in the XRD analysis. Figure 3 (g and h) illustrates the effect of 5.6 KV electric potential on the deposited film. It can be clearly noticed that the applied 5.6 KV electric potential leaded to the formation of random sheets with cluster size range of $136 - 337\ nm$, while the average particle size and the film thickness were 6.35 ± 0.03 and $498.35\ nm$, respectively. The size decreases with the increase of the applied potential due to the constant breakage of the droplets along the spray path [22]. The elemental's percentage as well as the purity of the utilized chemicals in the deposition of C_{60} films using the different effects of the electric potential are demonstrated (inset in Figure 3). All deposited C_{60} films contain two dominant peaks which are well corresponded to the presence of C and O elements. The attained C signal is mainly attributed to the carbon exists in the final deposited film with a high percentage, while the O signal is attributed to the absorbed of oxygen. However, there is an insignificant trace of gold (Au) which is resulted due to the FESEM sample preparation process.

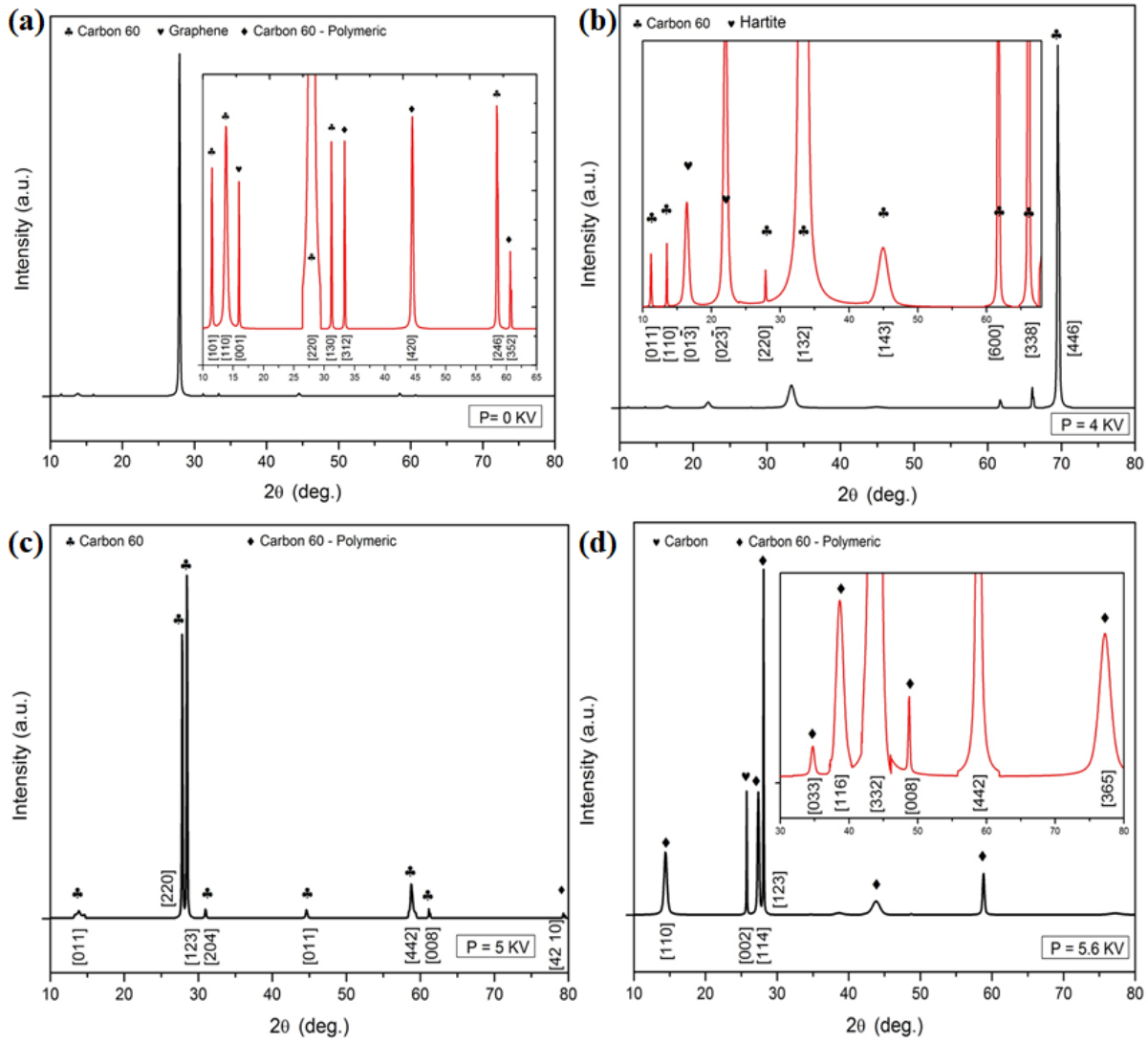

Figure 2. XRD patterns of the deposited films under (a) 0 KV, (b) 4 KV, (c) 5 KV, and (d) 5.6 KV.

Table 1. The structural parameters as a function of the applied electric potential.

Potential (KV)	Av. Cyst. Size(nm)	crystallinity indices
0	113.4	98.9
4	64.95	93.2
5	90.34	87.8
5.6	41.46	96.8

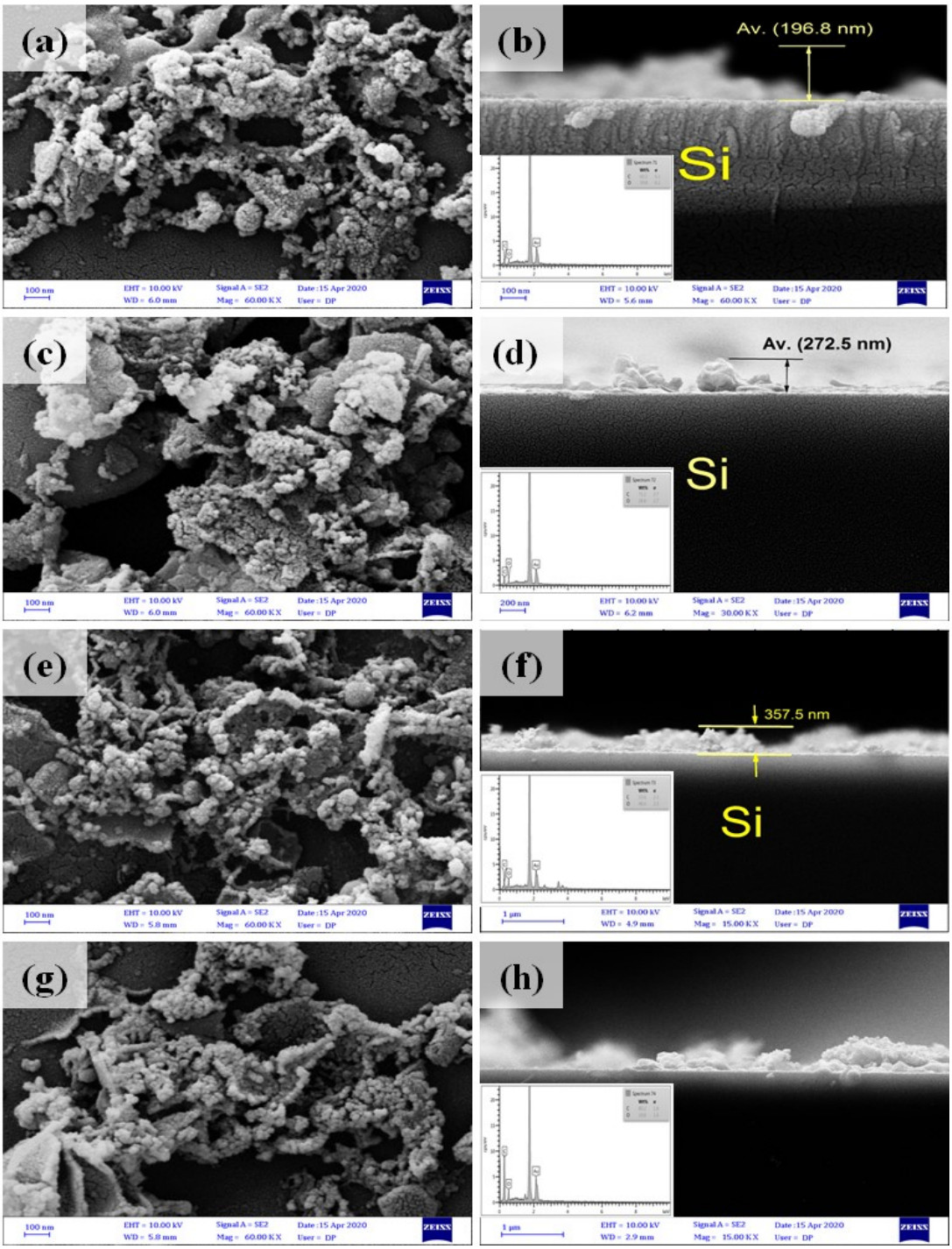

Figure 3. Top-view and cross-section FESEM analysis of the deposited films under different electric potential values; (a) free potential top-view, (b) free potential cross-section, (c) 4 KV top-view, (d) 4 KV cross-section, (e) 5 KV top-view, (f) 5 KV cross-section, (g) 5.6 KV top-view, (h) 6.5 KV cross-section.

The optical behavior of the reported films as a function of different electric field effect was studied using photoluminescence (PL) technique as depicted in Figure 4 (a-d). Hypothetically, PL emission spectra can be classified as two main regions; one of which, so-called NBE, is originated from the photo-generated electron transition from conduction band (CB) to the valence band (VB). While the second PL emission spectra is originated from the defect states of electron transition, so-called DLE [23].

In general observation, the PL spectra of the prepared films exhibited a NBE emission at above 1.7 eV evidencing the emission transition of electron from the conduction band. In particular, the PL peaks locations are to some extent shifted upon higher applied electric field; this could be attributed to the weak C_{60} solids inter-molecular bonds [24]. The major domination of the emission line in this region is due to the self-trapped polaronic exciton radiative recombination. This particular complex exciton happens because of the strong coupling of electron-vibration in the clusters of C_{60}. Continuously, the stated excitation is localized and also could be a trapped Frenkel exciton by the dislocation of lattice [10]. Moreover, the deposited film under free potential showed four clearly sub-bands in de-convoluted Gaussians at 1.742, 1.754, 1.769, and 1.786 eV, respectively. Whereas, the prepared films under 4 KV of potential demonstrated two clearly sub-bands at 1.76 and 1.79 eV as shown in Figure 4 (b) (red dashed line) with levels separation of 27.4 meV. Furthermore, three Gaussians peaks were emerged at 1.731, 1.76, and 1.8 eV with 29, and 40 meV of separation for the prepared films with potential of 5 kV, respectively. The prepared films under 5.6 kV of potential demonstrated one peak at 1.797 eV which is similar to the findings reported by Bayramov et al. [24]. It should be mentioned that the PL spectrum of the prepared C_{60} films, demonstrated in Figure 4, are in an upright agreement with previous reports [10,25].

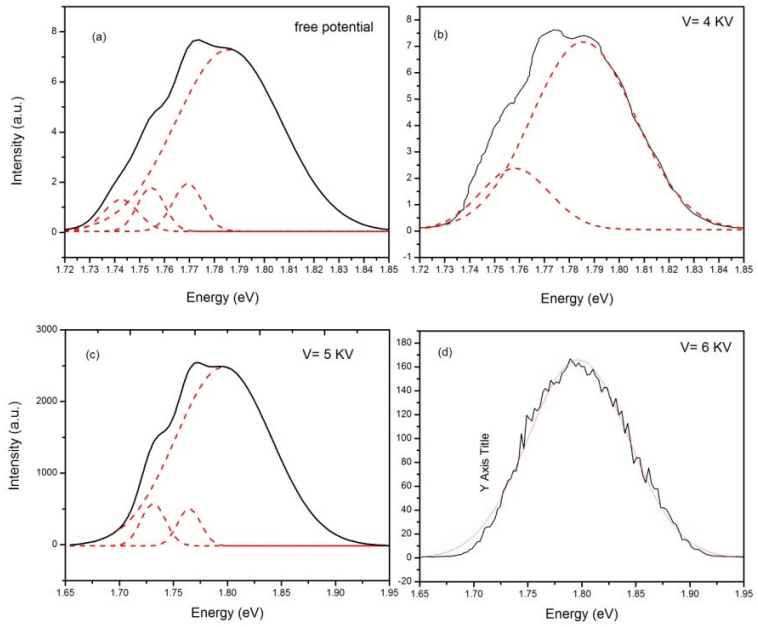

Figure 4. Photoluminescence spectra of C_{60} films at different electric field effect.

4. Conclusion

The fullerenes (C_{60}) thin film was successfully prepared using a combination of laser pulsed and electrospray approaches using wasted batteries' electrodes as precursor. The structural, morphological, and optical properties of the deposited films were in detail studied. The crystallite size, obtained from the XRD results, revealed an average size ranging from 41.46-111.84 *nm*. The effect of the applied electrical field was clearly elaborated through the XRD analysis as well as the surface analysis; where a particle size of 7.4 *nm* was attained under free potential. In the meanwhile, during 5.6 KV effect, the estimated particle size reduced to 5.35 *nm*. The presented results suggest the usefulness of the electric field effect during the deposition process for future optoelectronic design.

References

[1] Saraswati T E, Setiawan U H, Ihsan M R, Isnaeni I and Herbani Y 2019 The Study of the Optical Properties of C_{60} Fullerene in Different Organic Solvents *Open Chem.* vol **17** no.1 pp. 1198–1212

[2] Fernandez-Delgado O, Puente-Santiago A R, Cano M, Giner-Casares J J, Metta-Magaña A J and Echegoyen L 2020 Facile synthesis of C_{60}-nano materials and their application in high-performance water splitting electrocatalysis *Sustain. Energy Fuels* vol **4** no. 6 pp. 2900–2906

[3] Yadav J 2018 Fullerene : Properties , Synthesis and Application *Res. Rev. J. Phys.* vol **6** no. 3 pp. 1-6

[4] Lvarez-Murga M A and Hodeau J L 2015 Structural phase transitions of C_{60} under high-pressure and high-temperature *Carbon N. Y.* vol **82** pp. 381–407

[5] Oliveras O 2010 Theoretical studies of the exohedral theoretical studies of the exohedral reactivity of fullerene compounds *Universitat de Girona*

[6] Mutalib M Abd, Rahman M A, Othman M H D, Ismail A F and Jaafar J 2017 Scanning Electron Microscopy (SEM) and Energy-Dispersive X-Ray (EDX) Spectroscopy in *Membrane Characterization Elsevier* B V pp. 161–179

[7] Zhang L L, Zhou R and Zhao X S 2010 Graphene-based materials as supercapacitor electrodes *J. Mater. Chem.* vol **20** no. 29 pp. 5983–5992

[8] Montellano A, Ros T Da, Bianco A and Prato M 2011 Fullerene C_{60} as a multifunctional system for drug and gene delivery *Nanoscale* vol **3** no. 10 p. 4035

[9] Kumar M and Raza K 2017 C_{60}-fullerenes as drug delivery carriers for anticancer agents: promises and hurdles *Pharm Nanotechnol* vol **5** pp. 169–179

[10] Nishinaga J, Aihara T, Yamagata H and Horikoshi Y 2005 Mechanical and optical characteristics of Al-doped C_{60} films *J. Cryst. Growth* vol **278** no.1–4 pp. 633–637

[11] Zheng Q, Li Z, Yang J and Kim J K 2014 Graphene oxide-based transparent conductive films *Prog. Mater. Sci.* vol **64** pp. 200–247

[12] Umemoto K, Takeda M, Tezuka Y, Doi M, Lyu B and Masuhara A 2018 Morphology Control of Nanocrystallized C_{60} Thin Films Prepared by Poor Solvent Immersion *Technologies* vol **6** no. 2 p. 51

[13] Brunetti F, Operamolla A, Castro-Hermosa S, Lucarelli G, Manca V, Farinola G M and Brown T M 2019 Printed Solar Cells and Energy Storage Devices on Paper Substrates *Adv. Funct. Mater.* vol **29** no. 21 p. 1806798

[14] Wang Q, Dong Q, Li T, Gruverman A and Huang J 2016 Thin Insulating Tunneling Contacts for Efficient and Water-Resistant Perovskite Solar Cells *Adv. Mater.* vol **28** no. 31 pp. 6734–6739

[15] Liu X, Zhang Y, Zhang X, Li R, and Hu W 2020 Continuous and highly ordered organic semiconductor thin films via dip-coating: the critical role of meniscus angle *Sci. China Mater.* vol **63** no. 7 pp. 1257–1264

[16] Rueda-Delgado D, Hossain I M, Jakoby M, Schwenzer J A, Abzieher T, Howard I A and Paetzold U W 2020 Solution-processed and evaporated C_{60} interlayers for improved charge transport in perovskite photovoltaics *Org. Electron* vol **77** p. 105526
[17] Mao S, Ortiz J, Wang O, Malinge J, Badia A A and Kena-Cohen A 2020 Langmuir-Blodgett Fabrication of Large-Area Black Phosphorus- C_{60} Thin Films and Heterojunction Photodetectors *Nanoscale*
[18] Palotás J, Martens J, Berden G and Oomens J 2020 The infrared spectrum of protonated buckminsterfullerene $C_{60}H^+$ *Nat. Astron.* vol **4** no. 3 pp. 240–245
[19] Jaworek A 2007 Electrospray droplet sources for thin film deposition *J. Mater. Sci.* vol **42** no. 1 pp. 266–297
[20] Ilyas S, Heryanto B Abdullah and Tahir D 2019 X-ray diffraction analysis of nanocomposite Fe_3O_4/activated carbon by Williamson–Hall and size-strain plot methods *Nano-Structures & Nano-Objects* vol **20** p. 100396
[21] Coll A 2010 Characterization of nanoparticles deposition with electrospray *Politècnica de Catalunya University*
[22] Tisserant J N, Wagner T, Reissner P A, Beyer H, Fedoryshyn Y and Stemmer A 2017 Visualizing Local Morphology and Conductivity Switching in Interface-Assembled Nanoporous C_{60} Thin Films *ACS Appl. Mater. Interfaces* vol **9** no. 32 pp. 27166–27172
[23] Nasr M, Viter R, Eid C, Warmont F, Habchi R, Miele P and Bechelany M 2016 Synthesis of novel ZnO/$ZnAl_2O_4$ multi co-centric nanotubes and their long-term stability in photocatalytic application *RSC Adv.* vol **6** no. 105 pp. 103692–103699
[24] Bayramov A I, Mamedov N T, Dzhafarov T D, Aliyeva Y N, Ahmadova K N, Alizade E H and Ragimov S K 2019 Photoluminescence and optical transitions in C_{60} fullerene thin films deposited on glass, silicon and porous silicon *Thin Solid Films* vol **690** no. May 2018 p. 137566
[25] Akimoto I and Kan'no K I 2002 Photoluminescence and Near-Edge Optical Absorption in the Low-Temperature Phase of Pristine C_{60} Single Crystals *J. Phys. Soc. Japan*